Development and Analytical Study of a High-Gain Boost Converter for Renewable Energy Systems

Vempada priyanka¹, Dadi kalavathi²

¹ PG Student, EEE & Sankethika Vidya parishad College of Engineering, Visakhapatnam

² Assistant professor OF EEE Department, EEE & Sankethika Vidya parishad College of Engineering, Visakhapatnam

ABSTRACT

DC-DC converters are becoming High-gain increasingly common in solar PV systems and renewable energy applications. This article presents a non-isolated, non-coupled inductor-based highgain DC-DC boost converter that offers high voltage gain at reduced duty ratios while ensuring low voltage stress on controlled power switches. The proposed converter is well-suited for boosting lowinput DC voltage from distributed generation sources, such as fuel cells or photovoltaic (PV) systems, to a significantly higher DC voltage. With just two switches controlled by a single PWM signal, the topology simplifies control, reduces weight, minimizes cost, and enhances compactness. To further optimize performance, a machine learningbased predictive algorithm using a paragraph model is integrated into the converter's control system. This model analyzes historical and real-time data to dynamically adjust the duty cycle, improving voltage regulation and efficiency under varying load and input conditions. By leveraging machine learning, the converter can predict optimal switching patterns, reducing losses and enhancing stability in renewable energy applications. A comparative analysis with existing high-gain boost converters demonstrates that the proposed model outperforms previous topologies across multiple performance metrics. A 300 W hardware prototype is developed and tested in a laboratory environment to validate the theoretical claims. The proposed topology achieves a high gain of approximately 12 times the input voltage, with a reduced duty ratio—11.25 at a duty cycle of 0.6 and 17.77 at a duty cycle of 0.7. Efficiency ranges between 92.5% and 94.5%, making it suitable for medium-to-high power applications. The integration of machine learning further enhances system adaptability and operational efficiency, making the converter an ideal solution for next-generation sustainable energy systems requiring high output voltage and improved performance.

I. OVERVIEW

When converting modest input direct current (DC) voltages, such as a few volts, to significantly higher DC voltage levels, high-gain DC-DC boost converters play a crucial role [1]. These converters must provide efficient voltage step-up while maintaining a stable input current. Applications for such converters include solar photovoltaic (PV) systems, electric vehicles, high-voltage DC systems, and robotics [2], [3]. For many residential and commercial applications, a relatively high output voltage is necessary, whereas energy sources like fuel cells and solar PV systems generate low DC voltage. This has led researchers to focus extensively on the development of high-step-up DC-DC converters to meet the growing demand. DCcomposed converters are of different configurations of inductors, capacitors, diodes, and switches, which facilitate energy exchange between inductors and capacitors. The process begins with inductors storing energy, followed by capacitors receiving and transferring this energy to achieve a higher output voltage level [4]. A DC energy system's schematic is illustrated in Figure 1, where a high-gain DC-DC converter regulates voltage levels in a DC microgrid. Modern DC microgrids supercapacitors and high-gain DC-DC converters to improve stability. Additionally, in islanded mode, these converters are often paired with inverters to serve alternating current (AC) loads efficiently. Due to their superior voltage conversion capabilities, highgain DC-DC converters are increasingly being adopted as alternatives to conventional boost converters and their derivatives [5]. Traditional DCboost converters, however, have certain limitations, such as excessive input current ripples, high voltage stress, increased electromagnetic interference (EMI), and reduced efficiency. To

overcome these challenges, a machine learning-based control is proposed. By leveraging historical and realtime data, the machine learning model dynamically adjusts the duty cycle and optimizes switching patterns to enhance voltage regulation, reduce losses, and improve overall efficiency. This predictive algorithm ensures better adaptability to varying input and load conditions, making the high-gain DC-DC converter more reliable and efficient for renewable energy applications. The integration of machine learning not only improves performance but also enables smart energy management, ensuring stability and higher efficiency in DC microgrid systems. Traditional DC-DC boost converters have certain limitations, such as excessive input current ripples, high voltage stress, increased electromagnetic interference (EMI), and reduced efficiency under light load conditions. As a result, they become unsuitable for real-world applications where the duty ratio exceeds a certain threshold. To address these challenges, is proposed. This model leverages realtime and historical data to optimize the converter's performance by dynamically adjusting the duty cycle and switching patterns. By predicting voltage fluctuations and load variations, the machine learning model enhances voltage regulation, reduces losses, and improves system efficiency. This intelligent approach ensures that the high-gain DC-DC converter remains highly efficient and stable across varying load conditions, making it more suitable for practical applications in renewable energy and DC microgrid systems.

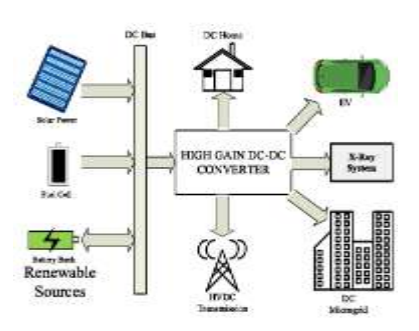


FIGURE 1. DC energy system.

Between the source and the load, DC-DC converters act as a bridge. Generally, these converters fall into two categories: isolated and non-isolated. When combined with microgrids, conventional boost converters, as shown in Figure 2(a), must operate at higher duty ratios, which subjects the converter to significant current and voltage stress. As the duty ratio increases, voltage gain and converter efficiency decrease due to the rise in parasitic resistance (ESR) in the capacitor and inductor. Non-isolated converters

can be further classified into coupled inductor and non-coupled inductor-based setups. In contrast, isolated converters electrically separate the load from the input power source using a high-frequency transformer, preventing direct current flow between them. However, this approach increases size and cost, making it less desirable for compact, cost-effective solutions [6,7,8,9]. For high-power applications requiring a shared ground between the source and load, isolated setups remain preferable. At lower duty ratios, coupled inductor configurations can achieve significantly high voltage gains. However, at higher duty cycles, they introduce challenges such as leakage inductance, conduction losses, lower efficiency, and switch voltage stress [10]. To address these issues, this study integrates a machine learning-based paragraph model to optimize converter performance. By analyzing real-time and historical operating data, the machine learning model predicts and adjusts control parameters dynamically, ensuring optimal switching patterns and improved duty cycle management. This predictive approach reduces energy losses, enhances voltage regulation, and minimizes stress components, resulting in higher efficiency and reliability. The integration of machine learning enables the converter to adapt to varied load and operating conditions, making it a more effective and intelligent solution for renewable energy systems and DC microgrids.

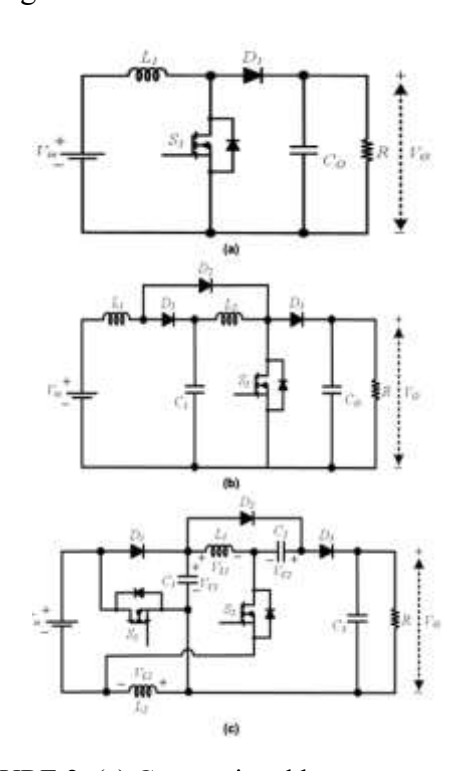


FIGURE 2. (a) Conventional boost converter (b)
Conventional quadratic boost converter (c) Proposed high
gain boost converter.

Non-coupled inductor topologies that are not isolated are often preferred when there is no requirement to isolate the input from the output. Non-isolated converters are widely used due to their simplicity, compact design, and cost-effectiveness. This article proposes several DC-DC converter topologies to address the limitations of conventional designs. A comparative analysis of multiple non-isolated high step-up DC-DC converters is presented in [11], highlighting their efficiency and performance tradeoffs. Additionally, various quadratic boost converter (QBC) topologies have been introduced in [12], [13], and [14]. These designs effectively reduce the stress on switching devices, allowing for significantly higher voltage gains at lower duty cycles. However, at higher duty ratios, the inductor core is more prone to saturation, leading to increased losses and reduced efficiency. To address these challenges, this study integrates a machine learning-based paragraph model to optimize quadratic boost converter performance. By utilizing real-time and historical data, the model dynamically adjusts duty cycles, switching patterns, and inductor current profiles, preventing core saturation and improving overall efficiency. Machine learning algorithms can predict inductor saturation levels, optimize control signals, and reduce inductor current ripples, enhancing the stability and reliability of the converter. This intelligent control strategy ensures improved voltage regulation, lower energy losses, and enhanced component longevity, making the proposed quadratic boost converter more efficient for high-voltage DC applications and renewable energy systems. The quadratic boost converter is depicted in [15], while a quasi-Z-source converter is demonstrated in [16] and [17]. This converter operates within a limited duty cycle range but replaces the inductor in a traditional high-gain boost converter with an impedance network, improving stability and voltage gain. Additionally, a boost converter with interleaving enhances output voltage and efficiency with fewer switches, as shown in [18]. A study in [19] presents an interleaved high-gain boost converter, which integrates two boost converters to achieve higher voltage conversion ratios. However, this design requires a large number of diodes and capacitors to maintain efficiency. A multiphase interleaved converter with a Z-source network eliminates the need for an input filter, achieving high gain with low input current ripple [20]. Furthermore, to enhance converter gain, a voltage boost circuit is added at the output stage. In [21], a voltage lift technique is applied to introduce a quadratic boost converter, while a highgain hybrid converter integrates voltage multiplier cells and switched capacitor cells to improve

efficiency and performance. To further optimize these converter topologies, this study integrates a machine learning-based paragraph model for adaptive control and efficiency enhancement. By analyzing real-time and historical data, the machine learning algorithm dynamically adjusts switching patterns, duty cycles, and impedance network parameters to optimize voltage conversion, reduce switching losses, and enhance stability. Additionally, predictive models can monitor component stress levels, capacitor chargedischarge behavior, and inductor saturation, allowing for proactive adjustments that prevent inefficiencies. This intelligent control approach enables higher voltage gains, reduced power losses, and improved reliability, making high-gain DC-DC converters more efficient and adaptable for renewable energy applications and DC microgrids.

Issues related to power device stress have been explored in [22]. A two-switch converter under varying voltage stress levels is presented in [23], which achieves high gain through a switching inductor voltage multiplier and a diode voltage capacitor multiplier. A non-isolated coupled inductor-based high step-up DC-DC converter with ultra-high voltage gain, made possible by an active switched inductor, is introduced in [24]. The three-winding linked inductor used in this design ensures a broad output voltage range, providing benefits such as wide voltage gain range for stability, minimal semiconductor spikes for reliability, and an easy-to-use gate driver control mechanism. This study proposes a non-isolated, noncoupled high-gain boost converter with a novel topology. The key advantages of the suggested converter include:

- High voltage gain and continuous current mode (CCM) operation, making it a suitable choice for medium- to high-power applications.
- The converter achieves a high gain of approximately 17.77 at a duty cycle of 0.7 and 11.25 at a duty of 0.6, presenting a viable and efficient solution.
- With an efficiency of approximately 92.5% to 94.5%, the proposed converter is well-suited for various renewable energy and DC microgrid applications.
- Despite using only two switches, the converter reduces voltage stress on power switches and operates with a single PWM signal, simplifying control and reducing gate driver requirements.

• The lack of a coupled inductor eliminates issues related to leakage inductance and switch stress at higher duty ratios.

To further optimize performance, this study integrates a machine learning-based paragraph model that dynamically adjusts switching patterns, duty cycles, and voltage multipliers to enhance efficiency, minimize losses, and improve voltage stability. By leveraging real-time data analysis, the machine learning model predicts optimal control parameters, ensuring reduced switching losses, improved component longevity, and stable operation under varying load conditions. This approach enables adaptive control, making the high-gain boost converter more efficient and intelligent for renewable energy and power electronics applications. The remainder of the paper is structured as follows:

- Section II explains the operation of the proposed converter.
- Section III compares the suggested high-gain boost converter with previously established topologies.
- Section IV presents the simulation results.
- Section V details the hardware implementation and outcomes.
- Section VI concludes the study.

II. SUGGESTED OPERATIONAL MODE AND CONVERTER

Figure 2(c) displays the schematic of a suggested high-gain boost converter. Two inductors (L1 and L2), three diodes (D1, D2, and D3), three capacitors (C1, C2, and C3), and two switches (S1 and S2) make up the converter. Both switches are operated by the same PWM signal. This lessens the need for gate driver circuitry and makes controlling the converter simpler. The suggested converter offers a viable way to attain high efficiency and benefit. It is appropriate for a wide range of medium-high power applications due to these appealing qualities. The next section explains the suggested converter's CCM and DCM modes of operation:

A.MODE OF CONTINUOUS CONDUCTION

There are two operating modes (switch on mode and switch off mode) that are determined by a switching signal. Both switches (S1 and S2) must be switched on and off at the same time for a converter to operate properly. When the CCM mode of operation is taken into account, both inductors (cap L sub 1 and cap L sub 2) must have regular current flow.

Additionally, the current across the inductor increases when energy is supplied from a source to both inductors.

Related waveforms for capacitor voltage and inductor current in a CCM mode are shown in Figure 3.

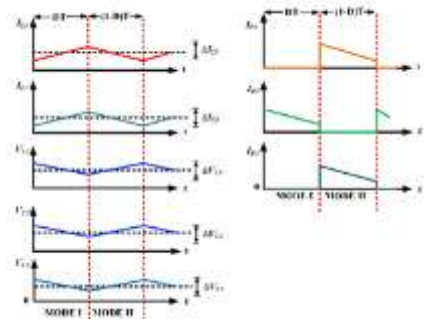


FIGURE 3. Related waveform in CCM mode. Zero \le t \le DT is Mode-1.

The diodes D1 and D3 become reverse biased and the diode D2 becomes forward biased in mode-1 when both switches S1 and S2 are activated. An comparable circuit design for a converter's initial operating mode is displayed in Figure 4. Kirchhoff's voltage law (KVL) was used to determine the switch-on mode equations in CCM (continuous conduction mode) for the analogous circuit below:

$$V_{L1} = V_{in} + V_{C2}$$

$$V_{L2} = V_{in}$$
(1)
(2)

FIGURE4. Equivalent circuit for switch-on mode of operation.

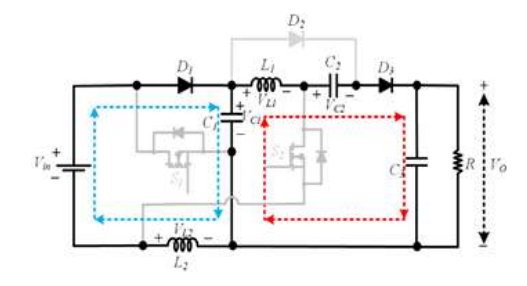
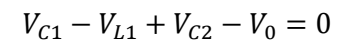


FIGURE5. Equivalent circuit for switch-off mode of operation.

2) Mode-2 (DT \leq t \leq T)

The analogous circuit in Figure 5 depicts the operation of the switch-off mode. In mode 2, the diodes D1 and D3 will conduct when switches S1 and S2 are switched off, while diode D2 will reverse bias and the energy stored in the passive component of the converter is transferred to the load. It is possible to obtain the equation for the second mode of operation by using the KVLtoane equivalent circuit.



$$-V_{L1} = V_0 - V_{C1} - V_{C2}$$
 (3)

4)

$$-V_{L1} = V_0 - V_{C1} - (V_{in} + V_{C1})$$

(5)

$$V_{L1} - V_{in} + 2V_{C1} - V_{0}$$

(6)

$$V_{L2} - V_{in} + V_{C1}$$

(7)

through the application of volt-inductor balance across an L2.

$$V_{in}D + (V_{in} - V_{C1})(1 - D) = 0 (8)$$

$$V_{C1} = \frac{V_{in}}{1 - D} \tag{9}$$

where VC1 is the converter's capacitor (C1) voltage. Vinist the converter's input voltage. Determine the pulsewidth modulation (PWM) gating signal's duty ratio. At the inductor L1, apply the voltage-inductor balance.

$$(V_{in} + V_{c1})D + (2V_{c1} + V_{in} - V_0)(1 - D) = 0$$

$$2V_{C1} - V_{C1}D + V_{in} - V_0(1-D) = 0$$

$$V_{C1}(2-D) - V_0(1-D) + V_{in} = 0$$
(11)

(12)

$$-V_0(1-D) + \frac{v_{in}(2-D)}{(1-D)} + V_{in} = 0$$

(13)

$$V_0(1-D) + \frac{2V_{in}-V_{in}D+V_{in}-V_{in}D)}{(1-D)}$$

(14)

$$V_0(1-D) + \frac{{}_{3}V_{in} - 2V_{in}D}{(1-D)}$$

(15)

$$\frac{V_0}{V_{in}} = \frac{(3-2D)}{(1-D)^2}$$

(16)

where V0 is the converter's output voltage. Vinist the converter's input voltage.

B. The method of discontinuous conductivity

Two requirements for a discontinuous conduction mode are shown in Figure 6. Any inconsistency in any of the participants The converter switches to the discontinuous conduction mode (DCM) due to currents. A generalized DC The following formulae can be used to calculate the suggested high gain converter:

$$V_{in}D_1 + (V_{in} - V_{C1})D_2 = 0$$

$$V_{in}D_1 + V_{in}D_2 = V_{C1}D_2 = 0$$

$$V_{C1} = \frac{V_{in}D_1 + V_{in}D_2}{D_2} \tag{18}$$

$$(V_{in} + V_{C1})D_1 + 2(V_{C1} + V_{in} - V_0)D_3 = 0$$

$$(V_{in} + V_{C1}D_1 + 2V_{C1}D_3 + 2V_{in}D_3 + 2V_0)D_3 = 0$$
(21)

$$(V_{in}D_1 = \left(\frac{V_{in}D_1 + V_{in}D_2}{D_2}\right)D_1$$

$$+2\left(\frac{V_{in}D_1+V_{in}D_2}{D_2}\right)D_3+2V_{in}D_3=2\frac{V_0D_3}{V_{in}}$$
(22)

$$\left(\frac{V_0}{V_{in}}\right)_{DCM} = \left(\frac{2D_1^2 + 4(D_1D_2 + D_1D_3 + D_2D_3)}{D_2D_3}\right)$$
(23)

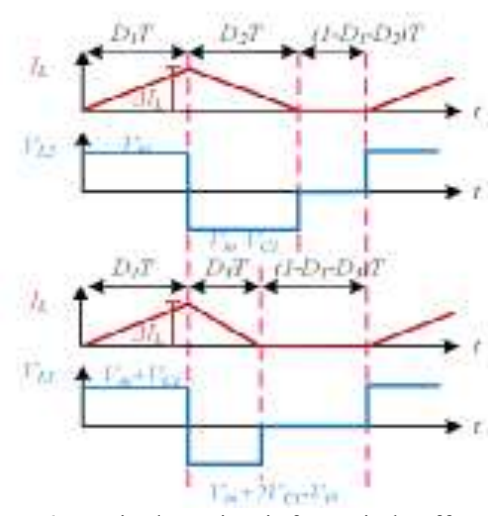


FIGURE6. Equivalent circuit for switch-off mode of operation.

C. Creating Components That Are Passive

The design and computation of passive elements are covered in detail in this section. The suggested converter must operate effectively in CCM mode, which requires careful design of the inductors and capacitors. A number of variables, including the duty ratio, output load, and switching frequency, affect the size of the passive components. Smaller component sizes are the result of higher switching frequency. 1) Calculating the Inductance Value The purpose of inductor design is to operate the

IJSREM | e-Journal

converter in CCM. The minimum needed inductance for L1 in CCM mode is specified by equation (30).

$$L_1 \frac{dI_{L1}}{dt} = V_{in} + V_{C1}$$

$$L_1 \frac{dI_{L1}}{dt} = V_{in} + \frac{V_{in}}{1 - D}$$
 (24)

$$L_{1} \frac{dI_{L1}}{dt} = \frac{V_{in} - V_{in}D + V_{in}}{1 - D}$$

$$L_{1} \frac{\Delta I_{L1}}{DT} = \frac{2V_{in} - V_{in}D}{2}$$
(25)

$$\frac{V_0}{R}L_1 \ge \frac{RV_{in}(2-D)DT}{2} \tag{27}$$

$$V_0 L_1 \ge \frac{RV_{in}(2-D)DT}{2}$$
 (28)

$$V_0 L_1 \ge \frac{RV_{in}(2-D)^2(2-D)D}{2(3-2D)f_S}$$

(30)

where D represents the duty ratio, f indicates the switching frequency, and R is the load value. List the inductor's necessary inductance (L1&L2).

Likewise, for inducer L2:

$$L_2 \geq \frac{R(1-D)^4D^2}{2f_s(3-2D)(1+D-D^2)}$$

(31)

2) CHOOSING THE THECAPACITY VALUE

The selection of a capacitor is based on the maximum permitted voltage ripple as well as the voltage across the capacitor. When choosing a capacitor and keeping it from exploding, its value should be considered. High enough to tolerate any possible high voltage that might be delivered across the capacitor. Using equation (37), the capacitor's value can be calculated.

$$I_{C1}\Delta T = C_1\Delta VC_1$$

$$I_{C1}\Delta T = C_1 \Delta V C_1 \tag{32}$$

$$\frac{V_o}{R(1-D)}C_1\Delta VC_1 \tag{33}$$

$$C_1 = \frac{V_o}{R(1-D)f_s\Delta V C_1} \tag{34}$$

$$VC_{1} = \frac{V_{in}(3-2D)}{(1-D)^{2}R(1-D)f_{s}\Delta VC_{1}}$$
(35)

$$C_1 = \frac{V_{in}(3-2D)}{R(1-D)^3 f_S \Delta V C_1}$$

(37)

Likewise, for capacitors C2 and C3:

$$C_2 = \frac{V_{in}(3-2D)}{R(1-D)^2 f_s \Delta V C_2}$$

$$C_3 = \frac{V_{in}(3-2D)}{R(1-D)^2 f_s \Delta V C_3}$$
 (38)

(39)

when the voltage is converted by Vinisthe. The switching frequency is fs. The acceptable ripple in the capacitor voltage is VC.

C1, C2, and C3 capacitors' required capacitance. ristheload value.

D. REALVOLTAGEGAIN

The efficiency is significantly impacted by parasitic factors such the on-state resistance of switches, diodes, and ESR of inductors and capacitors. Equation (43) provides the formula for determining the voltage gain while taking the converter's inductor ESR into account. The ideal and actual gain curves of a suggested topology are displayed in Figure 7

$$V_{in} \frac{V_o(3-2D)}{R(1-D)^2} = \frac{V_o^2}{R^2(1+D)^2} r L_1 + \frac{V_o^2(1+D-D^2)^2}{R^2D^2(1-D)^4} r L_2$$
(40)

$$\frac{V_{in}(3-2D)}{(1-D)^2} = V_0 \left(1 + \frac{r_{L1}}{R(1+D)^2} + \frac{(1+D-D^2)^2 r_{L2}}{RD^2 (1-D)^4}\right)$$

$$\frac{V_{in}(3-2D)}{(1-D)^2} = V_0 \left(\frac{RD^2(1-D)^4 + r_{L1}D^2(1-D)^2(1-D)^2 r_{L2}(1+D-D^2)^2}{RD^2(1-D)^2} \right)$$
(42)

$$V_0 = \frac{V_{in}(3-2D)RD^2(1-D)^2}{RD^2(1-D)^2r_{L2}(1+D-D^2)^2}$$

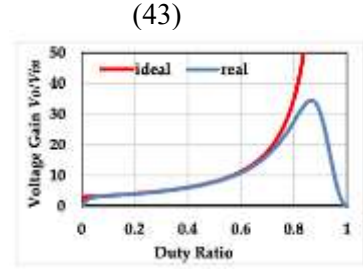


FIGURE 7. Ideal Vs real gain curve of a proposed topology.

TABLE 1. Comparison with other recent topologies.

-	Political	Aug.	Highway 18-1	Teacher .	-	- trapin	-
-	4.	. 1	2	+		2%	1-0%
100	2.	,	181	1.	14	1270	511 (S1814)
-	1	1		1		1100	2017
-		1				elle.	1,120
-	1	1	Ψ.	1.11	-	ris .	Ör.
-	1	- 1		1	-	117	elle.
	1	ű,	17	10		140	1-856
	+	0	9	45		21 Gal	1 - Marie 1 - Marie
œ	1	7	. * .	1.1	4	376	-
Approx.	A	1.		1.0	4.	rine .	
-	1		100	**		1:0	A PERSONAL PROPERTY.

© 2025, IJSREM | https://ijsrem.com

III. EXAMINATION OF OTHER NEW TOPOLOGIES COMPARISON OF DIFFERENT CONTROL SYSTEMS.

A. PERFORMANCE OF OPEN-LOOP

The simulation-designed parameters of a suggested converter are displayed in TABLE 2. This section discusses the simulation results of a suggested converter at various duty ratio settings.

TABLE 2. Simulation design parameters.

Parameters	Specifications		
Input voltage	$V_{to} = 24 \text{V} \sim 36 \text{V}$		
R_L Load	$R = 500 \Omega$		
Frequency	200 kHz		
Inductors L ₁ & L ₂	$L_1 = 24.5 \mu H$, $L_2 = 1 mH$		
Capacitors C ₁ , C ₂ & C ₃	$C_I = 33 \mu F$, $C_2 = 220 \mu F$, $C_3 = 220 \mu F$		
Duty Ratio	0.4, 0.6 and 0.7		

The simulation result of the suggested converter with a 24 V input is displayed in Figure 10(a). A 500 ohm load resistance and a duty ratio of 0.4 are used. 140 V is found to be the observed output voltage. Additionally, it is determined that the voltage across capacitors C1 and C2 is 40 V and 60 V, respectively. A simulation result with the same load resistance and input voltage at a duty ratio of 0.6 is displayed in Figure 10(b). It is found that the measured output voltage is 140 V. Following that, it is discovered that the voltages across capacitors C1 and C2 are, respectively, 58 V and 80 V. The results of the simulation at 36Vinput are displayed in Figure 10(c). The load resistance was 500 ohms, and the duty ratio was set at 0.7. 610 V is found to be the observed output voltage. About 110 V is the observed voltage of capacitor (C1), and 140 V is the voltage of capacitor (C2). The simulation result of the capacitor current waveform (C1, C2, and C3) is displayed in Figure 11(a). Figure 11 (b) displays the simulated waveforms for the diode current (ID1, ID2, and ID3) and switch current (ISW1, ISW2), respectively.

B. PERFORMANCE OF CLOSED-LOOP

A schematic design of the circuit that controls the recommended circuit output voltage is displayed in Figure 12. The suggested converter's closed-loop simulation performance is shown in Figures 13 and 14. The output voltage (Vo) is efficiently managed at 400 volts when the input voltage falls between 24 and 30 volts. Likewise, when the resistance to the load

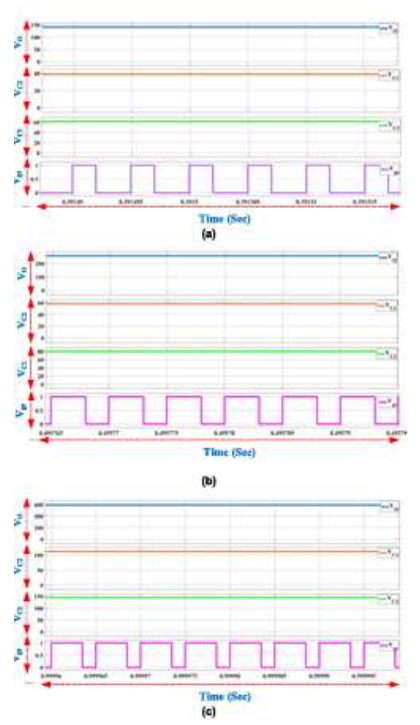


FIGURE 10. Simulation waveforms (VO,VC1 and VC2) of a proposed converter at a duty ratio of (a) 0.4, (b) 0.6, and (d) 0.7.



FIGURE 11. Current waveforms (a) Diode, (b) Capacitor, and (c) Switch

is changed, the PI controller keeps the output voltage constant. The output voltage stays steady at 400 V even when the load varies, demonstrating that the PI controller is operating as intended. The integral constant (Ki) and proportional constant (Kp) for the PI controller are given particular values.

Here, Ki is set at 0.02 and Kp is set at 0.05.

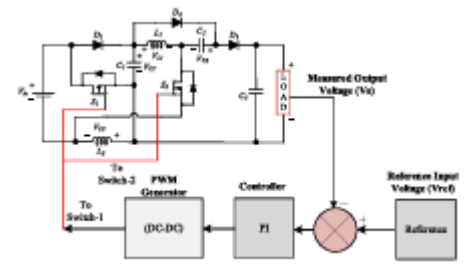


FIGURE 12. A schematic diagram of the closed loop control circuit.

International Journal of Scientific Research in Engineering and Management (IJSREM)

Volume: 09 Issue: 10 | Oct - 2025 SJIF Rating: 8.586 ISSN: 2582-3930

I used an STM32G474 microcontroller to target the gate driver circuit.

Two separate voltage regulator integrated circuits (MCWI03 48S15) and the converter switches are powered by the same DC power supply. The oscilloscope made by Tektronix (MDO3024) is used to

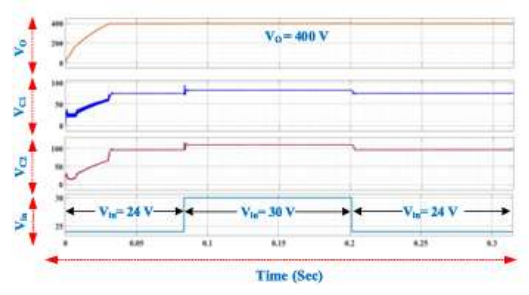


FIGURE 13. Simulation waveforms of output voltage with change in input voltage from 24 V to 30 V.

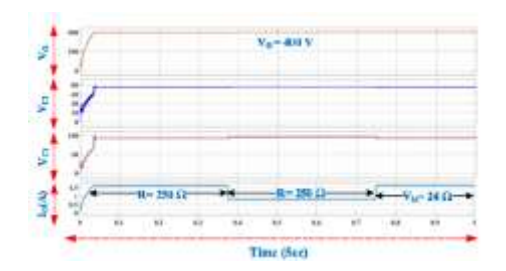


FIGURE 14. Simulation waveforms of output voltage with change in load resistance from 250 to 500.

document the results of a suggested open-loop converter performance.

The experimental waveforms of a suggested high-gain boost converter are displayed in Figure 17. The converter's output voltage (VO) and voltage stress waveforms across the switch (Vds1 and Vds2) are shown in Figure 17(a). According to the computed voltage gain, the output voltage at D = 0.6 and Vin = 24 V is found to be 280 V. The voltage stress across switches S1 and S2 is found to be 70 V and 180 V, respectively, based on the waveform that was caught. This is far less than the output voltage VO.

Parameters	Specifications			
Input voltage	V ₂₀ =24V - 36V			
Maximum power	P _{m0} = 300 W			
R. Lond	R = 500 Cl			
Frequency	200 kHz			
Inductors L. & L.	$L_1 = 24.5 \mu H$, $L_2 = 1 mH$			
Capacitons C ₁ , C ₂ & C ₃	$C_1 = 33 \mu F$, $C_2 = 220 \mu F$, $C_3 = 220 \mu F$			
Power MOSFET (S_1, S_2)	SPWS2N50C3, 560 V, 52 A, 0.07 Ω			
Diode $(D_1 - D_3)$	CMPFCD86-600V, I _F = 8 A, V _F + 1.5 V			
Microcontroller	STM32G474			
Gate driver IC	TLP250H			
Voltage regulator IC	MCWI03-48S15			
DC power supply	Chroma, 62100H-600S			

CONCULSION

The proposed high-gain boost converter achieves a voltage gain exceeding twelve times at a duty ratio of 0.6, making it a highly efficient solution for renewable energy applications. The absence of a coupled inductor reduces losses, minimizes electromagnetic interference (EMI), and makes the converter lighter

and more compact. This design maintains a high efficiency of approximately 94.5% at an input voltage of 24V, making it suitable for medium-to-high power applications. A hardware prototype of the proposed model was developed following a comprehensive with proper component steady-state analysis, selection, circuit design, and PCB layout optimization.

REFERENCES

[1]N.Subhani,Z.May,Md.K.Alam,I.Khan,M.A.Hossain,an dS. Mamun, "An improved non-isolated quadratic DC-DC boost converter with ultra high gain ability," IEEE Access, vol. 11350–11363, 2023. 11, pp. 10.1109/ACCESS.2023.3241863.

[2] R. V. Damodaran, H. Shareef, K. S. P. Kiranmai, and R. Errouissi, "Two-switch boost converter with improved voltage gain and degree of freedom of control," IEEE 23827–23838, 2023, Access, vol. 11, pp. 10.1109/ACCESS.2023.3249107.

[3] S. Pirpoor, S. Rahimpour, M. Andi, N. Kanagaraj, S. Pirouzi, and A. H. Mohammed, "A novel and high-gain switched-capacitor and switched-inductor-based DC/DC boost converter with low input cur rent ripple and mitigated voltage stresses," IEEE Access, vol. 10, pp. 32782–32802, 2022, doi: 10.1109/ACCESS.2022.3161576.

[4] M. A. Al-Saffar and E. H. Ismail, "A high voltage ratio and low stress DC-DC converter with reduced input current ripple for fuel cell source," Renew. Energy, vol. 82, pp. 35–43, Oct. 2015, doi: 10.1016/j.renene.2014.08.020. [5] M. Forouzesh, Y. P. Siwakoti, S. A. Gorji, F. Blaabjerg, B. Lehman, "Step-up and DC-DCconverters: Acomprehensivereview of voltage-boosting

Power Electron., vol. 32, no. 12, pp. 9143–9178, Dec. 2017. [6] F. Blaabjerg and D. M. Ionel, "Renewable energy devices and systems—State-of-the-art technology, research and development, chal lenges and future trends," Electric Power Compon. Syst., vol. 43, no. 12, pp. 1319–1328, Jul.

techniques, topologies, and applications," IEEE Trans.

[7] A. Allehyani, "Analysis of a transformerless single switch high gain DC-DC converter for renewable energy systems," Arabian J. Sci. Eng., vol. 46, no. 10, pp. 9691-9702, Oct. 2021, doi: 10.1007/s13369-021 05472-3.

[8] M. Rezvanyvardom, A. Mirzaei, M. Shabani, S. Mekhilef, M. Rawa, A. Wahyudie, and M. Ahmed, step-up soft-switching DC-DCboost "Interleaved converter without auxiliary switches," Energy Rep., vol. 8, 6499-6511, Nov. 2022, 10.1016/j.egyr.2022.04.069.

[9] L. Yang, W. Yu, and J. Zhang, "High voltage gain ratio isolated resonant switched-capacitor converter sustainable energy," IEEE Access, vol. 7, pp. 23055-23067, 2019, doi: 10.1109/ACCESS.2019.2893981.

[10] S.-W. Seo, J.-H. Ryu, H. H. Choi, and J.-B. Lee, "Input-parallel output-series high step-up DC/DC converter with coupled inductor and switched capacitor," IEEE Access, vol. 11, pp. 89164-89179, 2023, doi: 10.1109/ACCESS.2023.3302350.

- [11] H. Tarzamni, H. S. Gohari, M. Sabahi, and J. Kyyrä, "Nonisolated high step-up DC-DC converters: Comparative review and metrics applicabil ity," IEEE Trans. Power Electron., vol. 39, no. 1, pp. 582-625, Jan. 2024, doi: 10.1109/TPEL.2023.3264172.
- [12] S. Khan, A. Mahmood, M. Tariq, M. Zaid, I. Khan, and S. Rahman, "Improved dual switch non-isolated high gain boost converter for DC microgrid application," in Proc. IEEE Texas Power Energy Conf. (TPEC), Feb. 2021, pp. 1–6.
- [13]J.Ahmad, M.Zaid, A.Sarwar, C.-H.Lin, M.Asim, R. Yadav, M. Tariq, K. Satpathi, and B. Alamri, "A new highgain DC-DC converter with continuous inputcurrent for DCmicrogridapplications,"Energies, vol. 14, no. 9, p. 2629, May 2021.
- [14] J. Ahmad, C.-H. Lin, M. Zaid, A. Sarwar, S. Ahmad, M. Sharaf, M. Zaindin, and M. Firdausi, "A new high voltage gain DC to DC con verter with low voltage stress for energy storage system application," Electronics, vol. 9, no. 12, p. 2067, Dec. 2020.
- [15] A. Kumar, Y. Wang, X. Pan, M. Raghuram, S. K. Singh, X. Xiong, and A. K. Tripathi, "Switched-LC based high gain converter with lower component count," IEEE Trans. Ind. Appl., vol. 56, no. 3, pp. 2816–2827, May 2020. [16] M. M. Haji-Esmaeili, E. Babaei, and M. Sabahi, "High step-up quasi-Z source DC-DC converter," IEEE Trans. Power Electron., vol. 33, no. 12, pp. 10563-10571, Dec. 2018.
- [17] P. Kumar and M. Veerachary, "Z-network plus switched-capacitor boost DC-DC converter," IEEE J. Emerg. Sel. Topics Power Electron., vol. 9, no. 1, pp. 791– 803, Feb. 2021.
- [18] A. Chub, D. Vinnikov, E. Liivik, and T. Jalakas, "Multiphase quasi-Z source DC-DC converters for residential distributed generation systems," IEEE Trans. Ind. Electron., vol. 65, no. 10, pp. 8361–8371, Oct. 2018.
- [19] M. Meraj, M. S. Bhaskar, A. Iqbal, N. Al-Emadi, and S. Rahman, "Interleaved multilevel boost converter with minimal voltage multiplier components for high-voltage step-up applications," IEEE Trans. Power Electron., vol. 35, no. 12, pp. 12816-12833, Dec. 2020.
- [20] S. Khan, M. Zaid, A. Mahmood, J. Ahmad, and A. Alam, "A single switch high gain DC-DC converter with reduced voltage stress," in Proc. IEEE 7th Uttar Pradesh Sect. Int. Conf. Electr., Electron. Comput. Eng. (UPCON), Nov. 2020, pp. 1–6.
- [21] F. M. Shahir, E. Babaei, and M. Farsadi, "Analysis and design of voltage lift technique-based non-isolated boost DC-DC converter," IET Power Electron., vol. 11, no. 6, pp. 1083–1091, May 2018.
- [22] A.M.S.S.Andrade, T.M.K. Faistel, R.A. Guisso, and A. Toebe, "Hybrid high voltage gain transformerless DC-DC converter," IEEE Trans. Ind. Electron., vol. 69, no. 3, pp. 2470-2479, Mar. 2022.
- [23] M. Zaid, S. Khan, M. D. Siddique, A. Sarwar, J. Ahmad, Z. Sarwer, and A. Iqbal, "A transformerless high gain DC-DC boost converter with reduced voltage stress," Int. Trans. Electr. Energy Syst., vol. 31, no. 5, May 2021, Art. no. e12877.

[24] H. S. Gohari, N. A. Mardakheh, H. Tarzamni, N. V. Kurdkandi, K. Abbaszadeh, and J. Kyyra, "Non-isolated ultra-high voltage gain coupled inductor-based DC-DC converter," IEEE Trans. Circuits Syst. II, Exp. Briefs, vol. 70, no. 12, pp. 4459–4463, Dec. 2023, 10.1109/TCSII.2023.3285169.

ISSN: 2582-3930

- [25] Y.Tang, D.Fu,T.Wang,andZ.Xu,"Hybrid switchedinductor converters for high step-up conversion," IEEE Trans. Ind. Electron., vol. 62, no. 3, pp. 1480–1490, Mar.
- [26] A. Sarikhani, B. Allahverdinejad, and M. Hamzeh, "A nonisolated buck boost DC-DC converter with continuous input current for photovoltaic applications," IEEE J. Emerg. Sel. Topics Power Electron., vol. 9, no. 1, pp. 804– 811, Feb. 2021.
- [27] S. Ahmad, M. Nasir, J. Dabrowski, and J. M. Guerrero, "Improved topology of high voltage gain DC-DC converter with boost stages," Int. J. Electron. Lett., vol. 9, no. 3, pp. 342–354, Jul. 2021.
- [28] Y.Cao, V.Samavatian, K. Kaskani, and H. Eshraghi, "A novel nonisolated ultra-high-voltage-gain DC-DC converter with low voltage stress," IEEE Trans. Ind. Electron., vol. 64, no. 4, pp. 2809–2819, Apr. 2017.
- [29] K. Varesi, N. Hassanpour, and S. Saeidabadi, "Novel high step-up DC-DC converter with increased voltage gain per devices and continuous input current suitable for DC microgrid applications," Int. J. Circuit Theory Appl., vol. 48, no. 10, pp. 1820–1837, 2020, doi: 10.1002/cta.2804.
- [30] S. S. Lee, B. Chu, C. S. Lim, and K. B. Lee, "Twoinductor non-isolated DC-DC converter with high step-up voltage gain," J. Power Electron., vol. 19, no. 5, pp. 1069-1073, 2019, doi: 10.6113/JPE.2019.19.5.1069.
- [31] M. H. Ibrahim, S. P. Ang, M. N. Dani, M. I. Rahman, R.Petra, and S. M. Sulthan, "Optimizing step-size of perturb & observe and incremental conductance MPPT techniques using PSO for grid-tied PV system," IEEE Access, vol. 11, pp. 13079–13090, 2023, doi: 10.1109/ACCESS.2023.3242979.